CrossMark

Determination of cosmological parameters from gamma ray burst characteristics and afterglow correlations

H. Zitouni[1] (iD) · **N. Guessoum[2]** · **W.J. Azzam[3]**

Abstract We use the correlation relation between the energy emitted by the GRBs in their prompt phases and the X-ray afterglow fluxes, in an effort to constrain cosmological parameters and aiming to construct a Hubble diagram at high redshifts, i.e. beyond those found with Type Ia supernovae.

We use a sample of 126 *Swift* GRBs, that we have selected among more than 800 long bursts observed until April 2015. The selection is based on a few observational constraints: GRB flux higher than 0.4 photons $cm^{-2} s^{-1}$ in the band 15–150 keV; spectrum fitted with simple power law; redshift accurately known and given; and X-ray afterglow observed and flux measured.

The statistical method of maximum likelihood is then used to determine the best cosmological parameters (Ω_M, Ω_Λ) that give the best correlation for two relations: (a) the Amati relation (between intrinsic spectral peak energy $E_{p,i}$ and the equivalent isotropic energy); (b) the Dainotti relation, namely between the X-ray afterglow luminosity L_X and the break time T_a, which is observed in the X-ray flux FX.

✉ H. Zitouni
zitouni.hannachi@univ-medea.dz

N. Guessoum
nguessoum@aus.edu

W.J. Azzam
wjazzam@sci.uob.bh

[1] PTEAM Laboratory, Faculté des sciences, Université Dr Yahia Fares, Pôle urbain, Médéa, Algeria

[2] Department of Physics, College of Arts & Sciences, American University of Sharjah, Sharjah, United Arab Emirates

[3] Department of Physics, College of Science, University of Bahrain, Sakheer, Bahrain

Although the number of GRBs with high redshifts is rather small, and despite the notable dispersion found in the data, the results we have obtained are quite encouraging and promising. The results obtained using the Amati relation are close to those obtained using the Type Ia supernovae, and they appear to indicate a universe dominated by dark energy. However, those obtained with the correlation between the break time and the X-ray afterglow luminosity is consistent with the findings of the WMAP study of the cosmic microwave background radiation, and they seem to indicate a de Sitter-Einstein universe dominated by matter.

1 Introduction

Gamma-ray bursts (GRBs) are the most powerful explosions in the universe, and they occur in galaxies that can be at the farthest reaches of the (observable) universe. They have so far been observed with redshifts up to $z = 9.4$, with hopes of reaching $z = 20$ with future satellite detectors, qualifying them as potential cosmological probes. Although GRBs are not standard candles, the discovery of several luminosity and energy correlations opened a new window of investigation in which GRBs could be used to probe cosmological models and cosmological issues, like the star formation rate.

Two GRB luminosity correlations were discovered in 2000. The first is a correlation between a burst's luminosity and the time lag between the arrival of hard and soft photons in the burst (Norris et al. 2000). The second is a correlation between a burst's luminosity and its "spikiness" or variability (Fenimore and Ramirez-Ruiz 2000). These two

correlations were then used to create a GRB Hubble diagram (Schaefer 2003). Other luminosity and energy correlations were soon discovered, such as: the Amati relation (Amati et al. 2002, 2008, 2009; Amati 2006) which relates the intrinsic spectral peak energy, $E_{p,i}$, to the equivalent isotropic energy, E_{iso}; the Yonetoku relation (Yonetoku et al. 2004) which is a correlation between $E_{p,i}$ and the isotropic peak luminosity, L_{iso}; the Ghirlanda relation (Ghirlanda et al. 2004, 2006, 2010) which is a correlation between $E_{p,i}$ and the collimation corrected energy E_γ; and the Liang-Zhang relation (Liang and Zhang 2005) which relates E_{iso} to both $E_{p,i}$ and the break time of the optical afterglow light curves, T_a.

Early attempts to use GRB correlations to constrain cosmological parameters, such as the matter density parameter Ω_M, faced several problems (Dai et al. 2004; Azzam and Alothman 2006a, 2006b). The first problem was the scatter in the correlations, which made it difficult to pin down the cosmological parameters. The second was the circularity problem, which refers to the fact that in order to calibrate the luminosity and energy correlations, one must assume a cosmological model in the first place. The third problem was the paucity of data points with the required input parameters, like the redshift and the spectral peak energy. For a detailed discussion of these issues, the reader is referred to the recent review by Amati and Della Valle (2013) and the detailed study by Dainotti et al. (2013b) who clearly demonstrate the importance of taking proper account of the circularity problem, which could, otherwise, affect the evaluation of the cosmological parameters by 10 to 13 %.

In recent years, a revived interest in GRB cosmology has taken place, perhaps due to the new abundance of high quality data. For instance, Petrosian et al. (2015) investigated the cosmological evolution of a sample of 200 *Swift* bursts and utilized the results they obtained to put constraints on the star formation rate. Another recent study (Wang et al. 2015, 2016) provides a thorough investigation of how GRBs can be employed to constrain cosmological parameters, dark energy, the star formation rate, the pre-galactic metal enrichment, and the first stars (Totani 1997; Wijers et al. 1998; Mao and Mo 1998; Mao 2010; Porciani and Madau 2001; Natarajan et al. 2005; Hopkins and Beacom 2006; Jakobsson et al. 2006; Dermer 2007; Daigne and Mochkovitch 2007; Coward 2007; Yüksel and Kistler 2007; Kistler et al. 2008; Dainotti et al. 2015b).

In this paper, we use a sample of 126 Swift GRBs to investigate the correlation between the energy emitted by GRBs in their prompt phase and their X-ray afterglow fluxes. GRB luminosity correlations necessarily include cosmological parameters through the dependence of the luminosity on the burst's distance. The goal is to utilize the correlation between burst parameters to infer the best distance function, thus constraining the cosmological parameters and

creating a Hubble diagram at redshifts that go beyond those found in Type Ia supernovae.

2 Data preparation

The data for the prompt gamma portion was collected from the two official NASA/*Swift* websites.[1,2] For the X-ray part of each burst, we used the data published by the *Swift* public website[3] (Evans et al. 2009).

Until 25.04.2015, *Swift*/BAT had observed 304 GRBs with determined redshift. These bursts include 184 ones with an X-ray counterpart observed by *Swift*/XRT. We eliminated two GRBs, GRB060708 ($z < 2.3$) and GRB090814 ($0.696 \leq z \leq 2.2$) because their redshifts are given very approximately. For consistency in our calculations, we only keep bursts that have a spectrum expressed by a single power law (PL) (Dainotti et al. 2016) and whose spectral index is given by the *Swift* public website.[4] According to (Sakamoto et al. 2011) the rule of $\delta_{\chi^2} = \chi^2_{PL} - \chi^2_{CPL} < 6$ means that the CPL does not improve significantly the fit, thus the PL can be chosen as an equally good fit.

With this constraint we are left with 152 GRBs. We then add two constraints: a duration longer than two seconds, to keep only long bursts, and fluxes greater than 0.4 ph cm^{-2} s^{-1} (Ghirlanda et al. 2015). Two other GRBs were eliminated due to lack of data on their X-ray fluxes, GRB120714B, GRB080330, and a third a third one, GRB131103A, because of the presence of a very intense flare at about 1000 s. In the end, we are left with a first sample of 139 GRBs.

3 Statistical correlation methods

We use the maximum likelihood method as described in D'Agostini (2005), Amati et al. (2008), Dainotti et al. (2013a, 2016) to determine correlation relations. The objective is to determine the parameters m and q when interpolating a set of N data points (x_i, y_i) by a straight line $y = mx + q$ with standard deviations σ_x and σ_y. Hence, in order to determine the parameters (m, q, σ_{int}), we follow the Bayesian approach of D'Agostini (2005) by maximizing the likelihood function $\mathcal{L}(m, q, \sigma) = \exp[-L(m, q, \sigma_{int})]$, such that

---

$$L(m, q, \sigma)$$

$$= \frac{1}{2} \sum_{i=1}^{N} \left[\ln \left(\sigma_y^2 + m^2 \sigma_x^2 + \sigma_{y,i}^2 + m^2 \sigma_{x,i}^2 \right) \right.$$

$$\left. + \frac{(y_i - mx_i - q)^2}{\sigma_y^2 + m^2 \sigma_x^2 + \sigma_{y,i}^2 + m^2 \sigma_{x,i}^2} \right], \qquad (1)$$

where $\sigma = \sqrt{\sigma_y^2 + m^2 \sigma_x^2 + \sigma_{y,i}^2 + m^2 \sigma_{x,i}^2}$. σ_x, σ_y, $\sigma_{y,i}$, and $\sigma_{x,i}$ represent the standard deviations corresponding respectively to x, y, x_i and y_i. Because the errors on x and y were unknown, D'Agostini (2005) choose $\sigma_x = 0$ and set $\sigma_y = \sigma_v$. This choice is justified by the fact that y depends on several hidden parameters, while x does not depend on any factor. This has recently been used by Wang et al. (2016) to justify the choice of $x = E_p$ and $y = E_{iso}$ instead of the reverse, because E_{iso} depends on the cosmological parameters.

In this work, since we know neither σ_x nor σ_y we replace $m^2 \sigma_x^2 + \sigma_y^2$ by σ_{int}, noting that the latter is called extrinsic scatter by Amati et al. (2008), Wang et al. (2016) and "intrinsic scatter" by Dainotti et al. (2013a, 2016). It replaces the sum of all Gaussian errors that may affect (x, y) and which might come from other non-observed variabilities.

From the expression of σ_{int}, it is clear that the latter depends on the slope M times σ_{int}. but practically speaking, in the minimization procedure for the function $-\ln \mathcal{L}$ with respect to M and σ_{int}, the corresponding best value of σ_{int} must be of the same order as $\sqrt{\sigma_{y,i}^2 + m^2 \sigma_{x,i}^2}$. Hence, it depends on M as long as $\sigma_{y,i}$ is not dominant. In this regard, and in the aim of minimization its value, we choose the dependent variable $y = f(x)$, which gives a slope m such that $|m| < 1$.

We may refer to the work of Dainotti et al. (2015b) in order to compare the values of σ_{int} obtained for different values of M and given in the two tables. In our work and our sample, with $y = L_X$ and $X = T_a$, we obtain $m = -1.4$ and $\sigma_{int} = 0.6$. However, if we take $y = T_a$ and $x = L_X$, we get $m = -0.46$ and $\sigma_{int} = 0.29$. Since smaller values of m result in smaller values of σ_{int}, we choose L_X as the x variable and T_a as the y variable. This may be one of the reasons for the choices made by Amati (2003) and Ghirlanda et al. (2004) in their correlations.

We note that the maximization of likelihood function is performed on the two parameters (m, σ_{int}), because the parameter q, called "intercept" is obtained analytically from:

$$q = \left[\sum \frac{y_i - mx_i}{\sigma_{int}^2 + \sigma_{y,i}^2 + m^2 \sigma_{x,i}^2} \right]$$

$$\times \left[\sum \frac{1}{\sigma_{int}^2 + \sigma_{y,i}^2 + m^2 \sigma_{x,i}^2} \right]^{-1} \qquad (2)$$

for each pair (m, σ_{int}).

For comparison, and in simple cases, we shall use the χ^2 statistical method, which is defined as follows:

$$\chi^2 = \sum_{i=1}^{N} \frac{(y_i - mx_i - q)^2}{\sigma^2}, \qquad (3)$$

where $\sigma = \sqrt{\sigma_{int}^2 + \sigma_{y,i}^2 + m \sigma_{x,i}^2}$.

This method has also been used by Amati and Della Valle (2013) to constrain the cosmological parameters. It gives the same results as the maximum likelihood method when the number of data points is large. Statistically, the maximum likelihood method is more reliable when the data set is small (Saporta 2011; Martin 2012).

4 Calculation of the energy $E_{iso,\gamma}$ of the prompt gamma emission

We calculate the total isotropic energy $E_{iso,\gamma}$ emitted by the burst during the prompt phase using the following expression (Cardone et al. 2011)

$$E_{iso,\gamma} = 4\pi D_L^2(z) S_b (1+z)^{-1}, \qquad (4)$$

where S_b is the bolometric fluence. This quantity is related to the observed one by (Schaefer 2007):

$$S_b = S \frac{\int_{1/(1+z)}^{10^4/(1+z)} E \Phi_S(E) dE}{\int_{E_{min}}^{E_{max}} E \Phi_S(E) dE}, \qquad (5)$$

where S (erg cm^{-2}) is the observed quantity corresponding to the fluence. The integral represents a correction term (Zitouni et al. 2014). $\Phi_S(E)$ is the mean spectral energy. (E_{min}, E_{max}) is the energy range corresponding to the observing instrument. The energy range of *Swift*/BAT is (15 keV, 150 keV). D_L is the GRB luminosity distance computed in terms of the redshift z,

$$D_L(z) = \frac{(1+z)c}{H_0 \sqrt{|\Omega_k|}} \sinh\left\{ \sqrt{|\Omega_k|} F(z) \right\},$$

$$F(z) = \int_0^z \frac{dz'}{\sqrt{(1+z')^2 (1+\Omega_M z') - z'(2+z') \Omega_\Lambda}}, \qquad (6)$$

assuming a standard cosmological ΛCDM model with $\Omega_k = \Omega_m + \Omega_\Lambda - 1$, neglecting the radiation density given by the parameter Ω_r. c is the speed of light, H_0 is the Hubble constant at the present time. The *sinn* function is the sin function if $\Omega_k > 0$, corresponding to a "closed universe", and the sinh function if $\Omega_k < 0$, corresponding to an "open universe". For a flat space, $\Omega_k = 0$, thus D_L simplifies to

$$D_L(z) = \frac{(1+z)c}{H_0} \int_0^z \frac{dz'}{\sqrt{\Omega_M (1+z')^3 + \Omega_L}}. \qquad (7)$$

5 Calculation of the luminosity $L_X(t)$ and the energy $E_{iso,XA}$ of the X-ray afterglow

The luminosity of the afterglow in the X-ray band, $L_X(t)$, corresponding to a time t measured from the detection of the prompt emission, is given by the following expression (Sultana et al. 2012):

$$L_X(t) = 4\pi D_L^2 F_X(0.3\text{–}10 \text{ keV}, t) \times K_c, \tag{8}$$

where $F_X(0.3\text{–}10 \text{ keV}, t)$ is the flux observed at the time t in the X-ray band. K_c is the K-correction for the spectral power law obtained for each afterglow (Evans et al. 2009; Dainotti et al. 2010, 2016; D'Avanzo et al. 2012):

$$K_c = \frac{(\frac{10}{1+z})^{2-\Gamma} - (\frac{2}{1+z})^{2-\Gamma}}{10^{2-\Gamma} - 0.3^{2-\Gamma}}, \tag{9}$$

where Γ is the measured spectral index. The X-ray afterglow energy is calculated by integrating over time from its first detection to its end.

$$E_{iso,XA} = \frac{4\pi D_L^2(z)}{1+z} \times K_c \int_{t_1}^{t_2} F_X(t)dt, \tag{10}$$

where t_1 and t_2 are the start and end times of the X-ray afterglow.

The X-ray afterglow luminosity corresponding to a time t is calculated from the observed flux at that time. In the *Swift*/XRT data, we find the X-ray afterglows observed at the start denoted by $F_{X,early}$ (erg cm^{-2} s^{-1}), those observed eleven hours later denoted by $F_{X,11}$, and those observed after 24 hours denoted by $F_{X,24}$.

6 Study of the different correlation relations

In Fig. 1 we have plotted the energy $E_{iso,X}$ emitted by the X-ray afterglow against the luminosity $L_{X,early}$. $E_{iso,X}$ was calculated for a flat universe ($\Omega_k = 0$, $\Omega_{\Lambda=0.7}$, $\Omega_M = 0.3$, $H_0 = 70$ km s^{-1} Mpc^{-1}). Using the χ^2 statistical method, we note that there is a good correlation between the two quantities, except for 13 bursts falling outside of the group: GRB060926, GRB060904B, GRB061110B, GRB070411, GRB070611, GRB070506, GRB080411, GRB090529, GRB090726, GRB091024, GRB100902A, GRB120909A, GRB140114A. This group is characterized by X-ray afterglow fluxes that either do not have breaks in their temporal profiles or have a hint of a break in a highly slanted plateau.

In the rest of our study, we thus limit our sample to 126 GRBs (the previous 139 minus these 13), as there is a good chance of finding a strong correlation for them.

With this sample of 126 GRBs, we study the correlation between the prompt gamma emission and the X-ray afterglow. In Fig. 2, we plot the isotropic X-ray afterglow energy, denoted by $E_{iso,XA}$ against the gamma isotropic emission, denoted by $E_{iso,\gamma}$. We confirm a correlation between
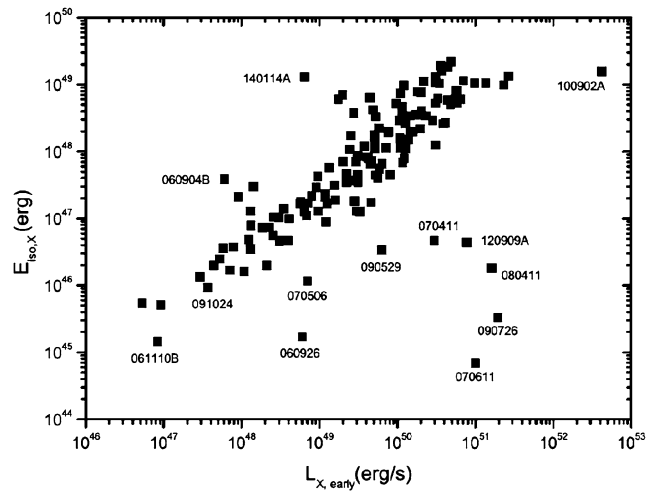

Fig. 1 Total isotropic X-ray afterglow energy $E_{iso,X}$ against the X-ray afterglow luminosity measured very early, denoted as $L_{X,early}$. ($\Omega_k = 0$, $\Omega_\Lambda = 0.7$, $\Omega_M = 0.3$, $H_0 = 70$ km s^{-1} Mpc^{-1})
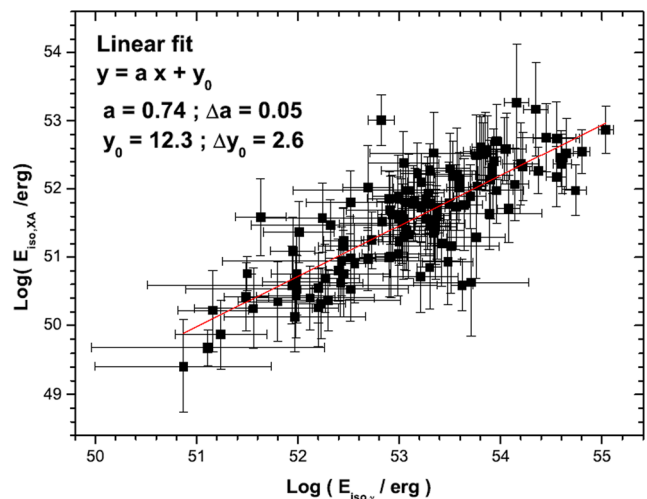

Fig. 2 Total X-ray afterglow isotropic energy, $E_{iso,XA}$, against the prompt emission isotropic energy, $E_{iso,\gamma}$, for our 126 GRBs

these quantities, which are obtained using the expressions (4) and (10). The first correlation relation is expressed analytically by the equation (11). We note that we find exactly the same slope as was found by Margutti et al. (2013). In a recent work, Zaninoni et al. (2016) find the following for long bursts: $m = 0.68 \pm 0.06$ and $y_0 = 16 \pm 2$, corresponding to $q = -0.64 \pm 0.08$. In our work, we obtain the following expression:

$$\log\left(\frac{E_{iso,XA}}{erg}\right) = (0.74 \pm 0.05) \log\left(\frac{E_{iso,\gamma}}{erg}\right)$$
$$+ (12.3 \pm 2.6). \tag{11}$$

In Fig. 3 we present a histogram of our 126 GRBs as a function of $\log(E_{iso,XA}/E_{iso,\gamma})$. We note that 67 GRBs (53
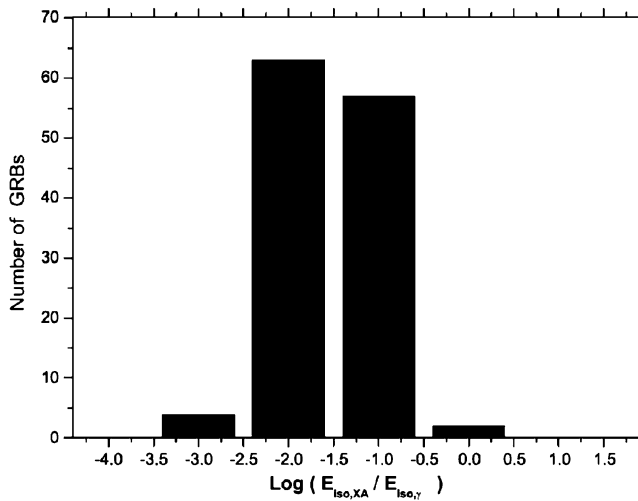
Fig. 3 Histogram of our 126 GRBs as a function of $\log(E_{iso,XA}/E_{iso,\Gamma})$ with a logarithmic step equal to 1

Fig. 4 Time profile of the X-ray afterglow flux of GRB150323A

% of the sample) have a ratio $r = (E_{iso,XA}/E_{iso,\gamma}) < 3$ %, and 124 of them (98.4 % of the sample) have $r < 30$ %. On average, we find $r = 0.03^{+0.07}_{-0.02}$. Considering the error box, this result is in agreement with the ratio of 10 % obtained by Willingale et al. (2007) and confirmed by Dainotti et al. (2015b).

Aiming to confirm a correlation relation between an observed quantity and an intrinsic source quantity, we have studied the correlation relations between $L_X(T_a)$, the X-ray afterglow luminosity determined at the time of the break T_a in the temporal profile of the X-ray flux after the plateau, and the break time T_a itself. We thus needed to determine those breaks in the X-ray flux time profiles, the latter being obtained from the *Swift* database *Swift*/XRT (Evans et al. 2009).

We should note that a correlation between T_a and $L_X(T_a)$ was found by Dainotti et al. (2008) based on a sample of 32 GRBs detected by *Swift*. The discovery of this relation has been the object of several updates based on newer sets of data (Dainotti et al. 2010, 2011, 2013a, 2013b, 2015a). These authors expressed L_X as function of the break time $T_a/(1 + z)$ in the source frame (the logarithmic variable $\log(T_a/(1 + z))$. Using the maximum likelihood estimator, Dainotti et al. (2015b) get $m = -0.90^{+0.19}_{-0.17}$ and $q = 51.14 \pm 0.58$ on a sample of 123 GRBs. In a recent work, Dainotti et al. (2016) add a third parameter, L_{peak}, and infer a new correlation plane from a total sample of 176 *Swift* GRBs. In our work, we have preferred to keep L_X as the independent variable and study a correlation with T_a.

Following that, we study the different possible correlations between the various intrinsic physical quantities obtained in the source's reference frame ($L_X(T_a)$, $E_{iso,XA}$, $E_{iso,\gamma}$) and the quantities observed by *Swift*/XRT, i.e. the break time T_a and the X-ray flux $FX(T_a)$. We also search
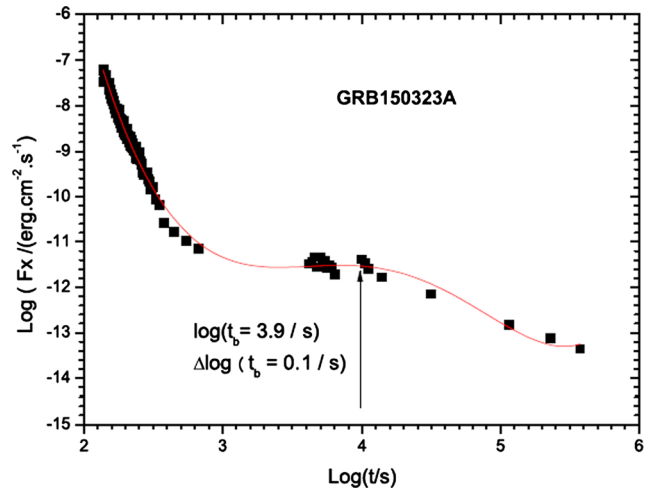
for a correlation between observed flux $FX(T_a)$ and intrinsic break time $T_a/(1 + z)$.

This study is performed on a sample of 73 GRBs, after having kept only those bursts with an X-ray flux that has a plateau followed by a break and which can be fitted by the phenomenological model given by Willingale et al. (2007).

In Table 1 we list the 73 GRBs with their redshifts and their characteristic quantities which we have calculated. The temporal profiles of these bursts more or less resemble those shown in Fig. 4, which presents the profile of the most recent GRB in our sample, i.e. GRB150323A.

To find the break time T_a and its uncertainty, we use the data given in the official Swift/XRT website,[5] which automatically treats the raw data; it classifies bursts into 5 types: (a) canonical; (b) one break, step first; (c) one break, shallow first; (d) no breaks; (o) oddball. Out of the 126 GRBs, we find 65 of type (a), 16 of type (b), 6 of type (c), 6 of type (d), and 31 of type (o). We use only the "canonical" ones (type a) and those that have a break after the X-ray flux plateau. We also add two bursts of type O, GRB100413A and GRB120729A, as their profiles are very similar to the (a) type. We thus end up with a sample of 73 bursts, given in Table 2.

In Fig. 5 we present the relation between the X-ray flux and the break time T_a for our sample of 73 GRBs. We confirm a correlation between the two quantities, and we express that with Eq. (12). This formula does not allow us to constrain the cosmological parameters, because both quantities are observed and independent of these parameters, but it does encourage us to try to confirm a correlation between T_a and the luminosity L_X at T_a.

We have thus sought such a correlation in a flat universe ($\Omega_k = 0$, $\Omega_\Lambda = 0.7$, $\Omega_M = 0.3$, $H_0 = 70$ km s^{-1} Mpc^{-1}).

---

[5]http://www.swift.ac.uk/xrt_live_cat/.

Table 1 Our sample consists of 73 GRBs, of which 65 are of type (a) canonical; 6 are of type (c) one break, shallow first; 2 are of type (o): oddball. Γ is the X-ray spectral index. The other quantities are defined in the text

GRB	z	Γ	$\text{Log}(\frac{E_{iso}}{\text{erg}})$	$\text{Log}(\frac{E_{iso,XA}}{\text{erg}})$	$\text{Log}(\frac{T_a}{\text{s}})$	$\text{Log}(\frac{FX(T_a)}{\text{erg cm}^{-2}\text{s}^{-1}})$	$\text{Log}(\frac{LX(T_a)}{\text{erg s}^{-1}})$
150323A[a]	0.593	2.06 ± 0.20	52.40 ± 0.12	50.81 ± 0.45	4.12 ± 0.35	−11.83 ± 0.19	45.15 ± 0.35
150314A[c]	1.758	1.85 ± 0.09	54.55 ± 0.10	52.18 ± 0.44	3.20 ± 0.14	−9.43 ± 0.02	48.69 ± 0.14
141121A[a]	1.470	1.93 ± 0.12	53.15 ± 0.27	51.82 ± 0.48	4.18 ± 0.06	−11.02 ± 0.12	46.92 ± 0.06
140907A[a]	1.210	2.01 ± 0.11	52.92 ± 0.16	51.01 ± 0.60	4.63 ± 0.25	−11.88 ± 0.02	45.86 ± 0.25
140703A[a]	3.140	1.83 ± 0.08	53.53 ± 0.19	52.19 ± 0.51	4.08 ± 0.14	−10.65 ± 0.05	48.03 ± 0.14
140419A[a]	3.956	1.87 ± 0.05	54.65 ± 0.11	52.52 ± 0.52	3.52 ± 0.36	−10.12 ± 0.14	48.81 ± 0.36
140304A[a]	5.283	2.02 ± 0.11	53.57 ± 0.23	52.22 ± 0.67	3.38 ± 0.44	−10.53 ± 0.53	48.77 ± 0.44
131103A[a]	0.599	2.19 ± 0.15	51.49 ± 0.22	50.42 ± 0.50	3.10 ± 0.47	−10.32 ± 0.24	46.65 ± 0.47
131030A[a]	1.293	2.10 ± 0.10	54.22 ± 0.09	52.33 ± 0.50	3.47 ± 0.38	−10.17 ± 0.15	47.65 ± 0.38
130831A[a]	0.479	1.79 ± 0.11	52.20 ± 0.04	50.55 ± 0.51	4.99 ± 0.07	−12.05 ± 0.14	44.72 ± 0.07
130606A[a]	5.913	1.87 ± 0.11	53.85 ± 0.22	52.55 ± 0.58	4.15 ± 0.43	−11.44 ± 0.28	47.88 ± 0.43
130514A[a]	3.600	2.06 ± 0.17	53.96 ± 0.05	52.70 ± 0.54	3.82 ± 0.76	−11.32 ± 0.69	47.60 ± 0.76
130505A[a]	2.270	1.92 ± 0.05	54.55 ± 0.23	52.74 ± 0.54	4.53 ± 0.21	−10.59 ± 0.05	47.80 ± 0.21
130418A[c]	1.218	1.69 ± 0.18	52.45 ± 0.20	51.24 ± 0.49	2.96 ± 0.35	−9.81 ± 0.24	47.90 ± 0.35
121211A[a]	1.023	2.07 ± 0.11	52.32 ± 0.78	51.47 ± 0.37	4.48 ± 0.33	−11.68 ± 0.17	45.88 ± 0.33
121128A[a]	2.200	1.98 ± 0.09	53.89 ± 0.52	51.64 ± 0.53	3.17 ± 0.14	−10.06 ± 0.09	48.32 ± 0.14
121027A[a]	1.773	2.37 ± 0.09	52.82 ± 0.13	53.01 ± 0.37	5.12 ± 0.12	−12.04 ± 0.04	46.16 ± 0.12
121024A[a]	2.298	2.01 ± 0.12	53.03 ± 0.62	51.49 ± 0.58	4.44 ± 0.56	−11.77 ± 0.40	46.66 ± 0.56
120729A[o]	0.800	1.88 ± 0.12	52.42 ± 0.22	50.62 ± 0.50	3.88 ± 0.12	−11.27 ± 0.02	46.03 ± 0.12
120404A[a]	2.876	1.90 ± 0.12	53.05 ± 0.11	51.30 ± 0.48	3.52 ± 0.37	−10.92 ± 0.32	47.71 ± 0.37
120327A[a]	2.810	1.76 ± 0.15	53.56 ± 0.14	51.74 ± 0.62	3.49 ± 0.27	−10.50 ± 0.04	48.05 ± 0.27
111228A[a]	0.716	2.04 ± 0.07	52.73 ± 0.11	51.25 ± 0.42	3.84 ± 0.13	−10.67 ± 0.17	46.50 ± 0.13
111123A[a]	3.152	2.56 ± 0.17	53.83 ± 0.12	52.51 ± 0.46	4.57 ± 0.35	−12.08 ± 0.08	46.84 ± 0.35
111008A[a]	5.000	1.94 ± 0.07	53.93 ± 0.07	52.41 ± 0.47	3.47 ± 0.24	−10.46 ± 0.10	48.75 ± 0.24
110801A[a]	1.858	2.05 ± 0.09	53.22 ± 0.14	52.10 ± 0.43	4.06 ± 0.39	−11.41 ± 0.18	46.80 ± 0.39
110213A[a]	1.460	1.96 ± 0.05	53.14 ± 0.18	51.79 ± 0.55	3.32 ± 0.41	−9.61 ± 0.02	48.32 ± 0.41
100906A[a]	1.727	2.03 ± 0.08	53.59 ± 0.04	52.14 ± 0.38	3.94 ± 0.10	−10.77 ± 0.17	47.36 ± 0.10
100814A[a]	1.440	1.89 ± 0.04	53.59 ± 0.12	52.02 ± 0.52	4.55 ± 0.11	−10.98 ± 0.20	46.93 ± 0.11
100704A[a]	3.600	2.12 ± 0.09	53.80 ± 0.08	52.61 ± 0.48	4.10 ± 0.28	−11.15 ± 0.24	47.79 ± 0.28
100621A[a]	0.542	2.30 ± 0.11	52.83 ± 0.03	51.52 ± 0.29	3.67 ± 0.41	−10.47 ± 0.26	46.38 ± 0.41
100615A[a]	1.398	2.38 ± 0.16	53.02 ± 0.05	51.61 ± 0.54	4.29 ± 0.18	−10.95 ± 0.09	46.97 ± 0.18
100425A[a]	1.755	2.17 ± 0.18	52.43 ± 1.18	50.94 ± 0.51	4.52 ± 0.70	−12.36 ± 0.39	45.81 ± 0.70
100418A[a]	0.624	2.27 ± 0.35	51.16 ± 0.35	50.22 ± 0.59	4.91 ± 0.28	−12.11 ± 0.06	44.90 ± 0.28
100413A[o]	3.900	1.96 ± 0.11	54.20 ± 0.18	52.37 ± 0.60	3.76 ± 0.42	−10.59 ± 0.27	48.37 ± 0.42
091020[a]	1.710	2.09 ± 0.07	53.26 ± 0.18	51.56 ± 0.54	3.90 ± 0.20	−10.95 ± 0.00	47.18 ± 0.20
090530[a]	1.266	2.04 ± 0.13	52.45 ± 0.46	50.76 ± 0.63	4.68 ± 0.58	−12.08 ± 0.32	45.71 ± 0.58
090516A[a]	4.109	2.09 ± 0.07	54.04 ± 0.08	52.59 ± 0.46	4.22 ± 0.10	−11.24 ± 0.14	47.83 ± 0.10
090418A[a]	1.608	2.03 ± 0.09	53.36 ± 0.21	51.45 ± 0.55	3.44 ± 0.21	−10.24 ± 0.02	47.81 ± 0.21
090113[c]	1.749	2.25 ± 0.23	52.52 ± 0.25	50.99 ± 0.61	2.78 ± 0.28	−10.23 ± 0.02	47.94 ± 0.28
090102[c]	1.547	1.77 ± 0.08	51.63 ± 0.25	51.59 ± 0.56	3.30 ± 0.49	−9.91 ± 0.44	48.06 ± 0.49
081008[a]	1.968	1.98 ± 0.11	53.29 ± 0.15	51.94 ± 0.40	4.27 ± 0.24	−11.41 ± 0.03	46.85 ± 0.24
081007[a]	0.529	2.10 ± 0.14	51.56 ± 0.58	50.25 ± 0.59	4.60 ± 0.33	−11.85 ± 0.10	45.00 ± 0.33
080928[a]	1.692	2.14 ± 0.10	52.90 ± 0.22	51.86 ± 0.39	4.35 ± 0.15	−11.64 ± 0.05	46.48 ± 0.15
080906[a]	2.000	2.00 ± 0.26	53.28 ± 0.23	51.79 ± 0.68	4.31 ± 0.48	−11.26 ± 0.28	47.02 ± 0.48
080905B[a]	2.374	1.86 ± 0.10	52.99 ± 0.25	51.89 ± 0.61	3.77 ± 0.56	−10.39 ± 0.34	48.03 ± 0.56
080810[a]	3.350	2.12 ± 0.10	53.92 ± 0.17	52.20 ± 0.56	3.80 ± 0.21	−10.76 ± 0.01	48.10 ± 0.21

Table 1 (*Continued*)

| GRB	z	Γ	$\mathrm{Log}(\frac{E_{iso}}{\mathrm{erg}})$	$\mathrm{Log}(\frac{E_{iso,XA}}{\mathrm{erg}})$	$\mathrm{Log}(\frac{T_a}{\mathrm{s}})$	$\mathrm{Log}(\frac{FX(T_a)}{\mathrm{erg\,cm^{-2}\,s^{-1}}})$	$\mathrm{Log}(\frac{LX(T_a)}{\mathrm{erg\,s^{-1}}})$
080707[a]	1.230	2.07 ± 0.19	51.98 ± 0.39	50.43 ± 0.61	4.18 ± 0.47	-11.89 ± 0.17	45.88 ± 0.47
080607[a]	3.036	2.03 ± 0.09	54.61 ± 0.09	52.37 ± 0.44	3.35 ± 0.37	-10.38 ± 0.16	48.35 ± 0.37
080430[a]	0.767	2.04 ± 0.08	51.99 ± 0.25	50.76 ± 0.61	4.51 ± 0.17	-11.58 ± 0.11	45.67 ± 0.17
080310[a]	2.427	2.09 ± 0.06	53.30 ± 0.48	52.27 ± 0.39	4.04 ± 0.11	-11.39 ± 0.15	47.12 ± 0.11
071021[a]	2.452	2.13 ± 0.13	52.91 ± 0.43	51.69 ± 0.50	4.43 ± 0.78	-11.87 ± 0.96	46.65 ± 0.78
070810A[c]	2.170	2.17 ± 0.16	53.30 ± 0.12	50.85 ± 0.61	3.80 ± 0.71	-11.54 ± 0.66	46.86 ± 0.71
070714B[a]	0.920	2.07 ± 0.15	52.30 ± 0.71	50.37 ± 0.45	3.42 ± 0.27	-11.10 ± 0.09	46.35 ± 0.27
070529[a]	2.500	1.98 ± 0.17	53.51 ± 0.48	51.16 ± 0.69	3.42 ± 0.54	-10.92 ± 0.35	47.59 ± 0.54
070318[a]	0.836	1.97 ± 0.10	52.69 ± 0.27	50.97 ± 0.46	5.43 ± 0.19	-12.60 ± 0.03	44.75 ± 0.19
070306[a]	1.497	1.94 ± 0.07	53.22 ± 0.23	51.72 ± 0.50	4.28 ± 0.16	-10.77 ± 0.14	47.19 ± 0.16
070208[c]	1.165	2.20 ± 0.19	51.80 ± 0.39	50.35 ± 0.58	3.12 ± 0.25	-10.96 ± 0.09	46.75 ± 0.25
070129[a]	2.338	2.28 ± 0.12	53.18 ± 0.17	52.23 ± 0.45	4.41 ± 0.22	-11.75 ± 0.22	46.76 ± 0.22
070110[a]	2.352	2.09 ± 0.06	53.06 ± 0.28	51.80 ± 0.57	3.54 ± 0.27	-10.62 ± 0.12	47.85 ± 0.27
061222A[a]	2.088	1.93 ± 0.06	53.90 ± 0.12	52.14 ± 0.58	4.83 ± 0.27	-11.41 ± 0.13	46.90 ± 0.27
061121[a]	1.314	1.90 ± 0.06	53.77 ± 0.09	52.04 ± 0.40	3.05 ± 0.20	-9.82 ± 0.14	48.00 ± 0.20
061021[a]	0.346	1.99 ± 0.06	52.23 ± 0.24	50.32 ± 0.52	4.61 ± 0.37	-11.47 ± 0.15	44.95 ± 0.37
060814[a]	0.840	2.12 ± 0.07	53.34 ± 0.09	51.36 ± 0.42	3.81 ± 0.36	-10.92 ± 0.05	46.43 ± 0.36
060729[a]	0.540	2.02 ± 0.04	52.01 ± 0.35	51.37 ± 0.45	4.49 ± 0.06	-10.79 ± 0.20	46.09 ± 0.06
060719[a]	1.532	2.57 ± 0.15	52.56 ± 0.11	50.91 ± 0.58	4.23 ± 0.61	-11.76 ± 0.41	46.27 ± 0.61
060714[a]	2.710	2.04 ± 0.11	53.26 ± 0.07	51.86 ± 0.51	3.67 ± 0.35	-11.18 ± 0.05	47.44 ± 0.35
060614[a]	0.130	1.90 ± 0.08	51.50 ± 0.04	50.76 ± 0.25	4.51 ± 0.14	-11.39 ± 0.12	44.09 ± 0.14
060607A[a]	3.082	1.61 ± 0.05	53.50 ± 0.20	52.30 ± 0.52	4.11 ± 0.05	-10.41 ± 0.13	48.17 ± 0.05
060605[a]	3.800	2.02 ± 0.09	52.99 ± 0.44	51.57 ± 0.61	3.77 ± 0.32	-11.00 ± 0.06	47.96 ± 0.32
060604[a]	2.136	2.17 ± 0.12	52.24 ± 0.58	51.58 ± 0.51	4.40 ± 0.20	-11.82 ± 0.11	46.57 ± 0.20
060526[a]	3.210	1.91 ± 0.12	53.04 ± 0.35	52.38 ± 0.46	4.33 ± 0.26	-11.03 ± 0.17	47.71 ± 0.26
060502A[a]	1.510	2.03 ± 0.12	53.04 ± 0.24	51.31 ± 0.63	4.44 ± 0.36	-11.50 ± 0.06	46.48 ± 0.36
060210[a]	3.910	2.08 ± 0.05	54.06 ± 0.19	52.59 ± 0.52	4.46 ± 0.17	-11.12 ± 0.07	47.90 ± 0.17
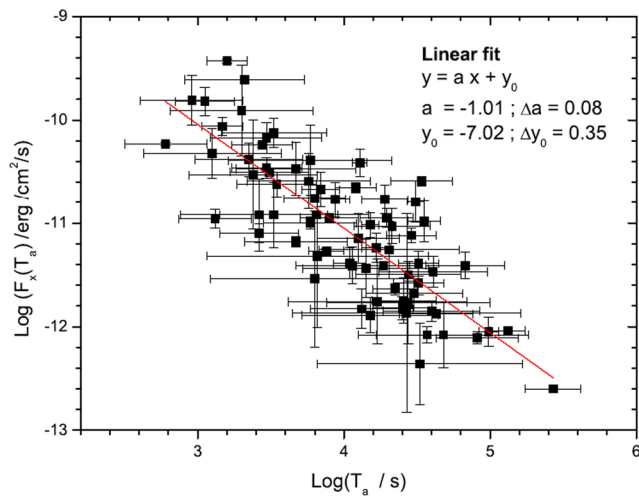
Fig. 5 X-ray flux calculated at the break time as a function of the break time T_a for 73 GRBs. ($\Omega_k = 0$, $\Omega_\Lambda = 0.7$, $\Omega_M = 0.3$, $H_0 = 70\ \mathrm{km\,s^{-1}\,Mpc^{-1}}$)

The correlation is shown graphically in Fig. 6 and analytically by Eq. (13). We note that these relations have rather good precisions, judging by the values of their slopes and intercepts (see the uncertainties on the power indices in Eqs. (12) and (13)).

$$F_X(T_a) = 10^{-7.02 \pm 0.35} T_a^{-1.01 \pm 0.08}, \tag{12}$$

$$\frac{T_a}{1 + z} = 10^{25.2 \pm 1.8} L_X(T_a)^{-0.46 \pm 0.04}, \tag{13}$$

with F_X in (erg cm^{-2} s^{-1}), T_a in seconds, and L_X in erg s^{-1}. z is the redshift and $T_a/(1 + z)$ is the break time measured in the source's rest frame.

We may compare with the recent work of (van Eerten 2014), who finds a slope of $-1.07^{+0.20}_{-0.09}$ for F_X as a function of T_a, which is quite close to our own result.

For that same sample of 73 GRBs we have studied the correlation between $L_X(T_a)$ and the isotropic energy of the prompt gamma emission, $E_{iso,\gamma}$. We present this relation graphically in Fig. 7 and analytically by Eq. (14). This rela-

tion has an uncertainty of 16 % on the slope and about 100 % on the value of the intercept:

$$L_X(T_a) = 10^{-5.5 \pm 6.0} E_{iso,\gamma}^{1.0 \pm 0.1}. \tag{14}$$

We note that this correlation relation suffers from a very large uncertainty on the value of the intercept, therefore it cannot be used to make any convincing inferences. By contrast, despite substantial scatter, the $L_X - T_a$ plot gives an intercept with only 10 % uncertainty. From the correlations that we have sought, we thus only retain the one between the break time T_a and the luminosity L_X at that time, with the goal of constraining cosmological parameters.
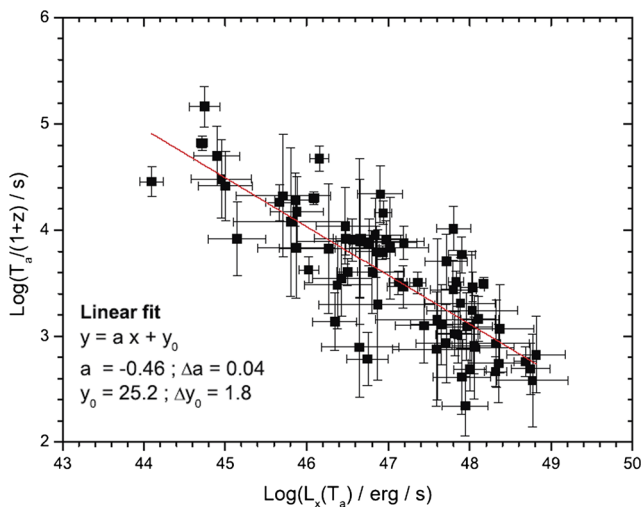
Fig. 6 Luminosity versus break time for 73 GRBs. ($\Omega_k = 0$, $\Omega_\Lambda = 0.7$, $\Omega_M = 0.3$, $H_0 = 70\,\mathrm{km\,s^{-1}\,Mpc^{-1}}$)
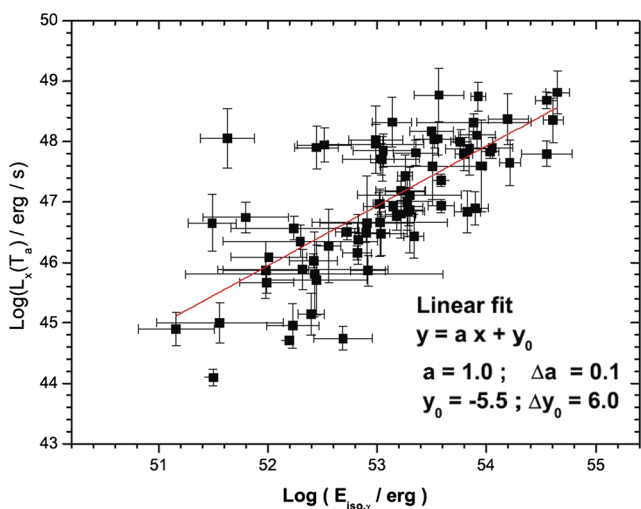
Fig. 7 X-ray afterglow luminosity, L_X, calculated at the break time as a function of $E_{iso,\gamma}$ for our sample of 70 GRBs. ($\Omega_k = 0$, $\Omega_\Lambda = 0.7$, $\Omega_M = 0.3$, $H_0 = 70\,\mathrm{km\,s^{-1}\,Mpc^{-1}}$)

7 Cosmological parameters derived from correlation relations

We use the maximum likelihood method as described in D'Agostini (2005), Amati et al. (2008), Dainotti et al. (2013a, 2016) to constrain the cosmological parameters within the standard ΛCDM model. We should note that in this work we try to constrain the cosmological constants Ω_Λ and Ω_M while taking a value $H_0 = 70\,\mathrm{km\,s^{-1}\,Mpc^{-1}}$ for the Hubble constant.

7.1 Usage of the Amati relation

We start by using the Amati relation, as presented in our previous work (Zitouni et al. 2014), in an effort to constrain the cosmological constant Ω_M. The Amati relation is given by the following equation:

$$\frac{E_{p,i}}{\mathrm{keV}} = K \times \left(\frac{E_{iso}}{10^{52}\,\mathrm{erg}} \right)^m, \tag{15}$$

where $E_{p,i}$ is the energy of the burst corresponding to the peak of the flux and measured in the source's frame, and E_{iso} is the total energy emitted by the source in all space. In this work, we use data for 27 bursts to infer the constants K and m (Zitouni et al. 2014), and we assume a flat universe, such that $\Omega_M + \Omega_\Lambda = 1$. It thus suffices to constrain one parameter to obtain the other.

Originally, the Amati relation was discovered for a flat universe, characterized by $\Omega_k = 0$, $\Omega_\Lambda = 0.7$, $\Omega_M = 0.3$, $H_0 = 70\,\mathrm{km\,s^{-1}\,Mpc^{-1}}$. These values were chosen based on the results obtained from SNe Ia data. In Table 2, we present the values of the m and q fitting parameters found in the framework of this model.

We stress that our novel approach consists in performing a "reverse job", namely to search for the cosmological parameters that give the best fit, which is when the likelihood function $-\ln \mathcal{L}$ is minimized. The fit is not given by specific values but rather by surfaces or contours corresponding to the same values of $-\ln \mathcal{L}$. We vary the cosmological constant Ω_M numerically between 0 and 1, and determine the values presented in Table 3 for the Amati correlation relation.

Table 2 Values of the slope m and intercept q. To compare with the original Amati relation, one must take $q = \log K - 52m$. Ref(1): Present work, Ref(2): Amati (2003), Ref(3): Ghirlanda et al. (2004). ($\Omega_k = 0$, $\Omega_\Lambda = 0.7$, $\Omega_M = 0.3$, $H_0 = 70\,\mathrm{km\,s^{-1}\,Mpc^{-1}}$)

m	q	σ_{int}	Ref.
0.37 ± 0.07	-15 ± 3	0.20 ± 0.01	(1)
0.35 ± 0.06	-16 ± 3		(2)
0.40 ± 0.05	-18.8 ± 2.7		(3)

Table 3 Best values obtained for the parameters of the Amati relation using the likelihood method. Data used here consist of 27 GRBs, taken from our previous work (Zitouni et al. 2014). Values are obtained assuming a flat universe ($\Omega_k = 0$), with Ω_M varying between 0 and 1 and $\Omega_\Lambda = 1 - \Omega_M$

Parameters	min	max
m	0.32	0.37
q	-17	-15
σ_{int}	0.19	0.21
$-\ln \mathcal{L}$	-25	-23.5
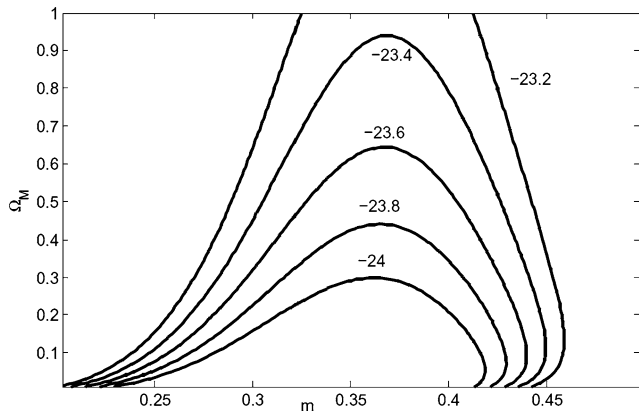
Fig. 8 The function $-\ln \mathcal{L}$ in the plane (m, Ω_M), with $\sigma_{int} = 0.20$ for the Amati relation obtained from the data for 27 GRBs of *Swift*/BAT (Zitouni et al. 2014). A contour represents the same value of $-\ln \mathcal{L}$ for different pairs of (m, Ω_M). We assume a flat universe, i.e. $\Omega_k = 0$
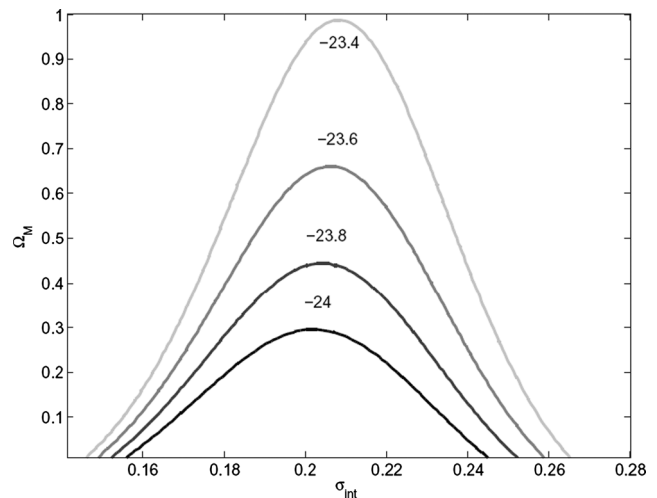

Fig. 9 The function $-\ln \mathcal{L}$ in the (σ_{int}, Ω_M) plane, with a slope $m = 0.37$, for the Amati relation obtained from the data for 27 GRBs in *Swift*/BAT (Zitouni et al. 2014). A *contour* represents the same value of $-\ln \mathcal{L}$ for different pairs of (σ_{int}, Ω_M). We assume a flat universe, i.e. $\Omega_k = 0$
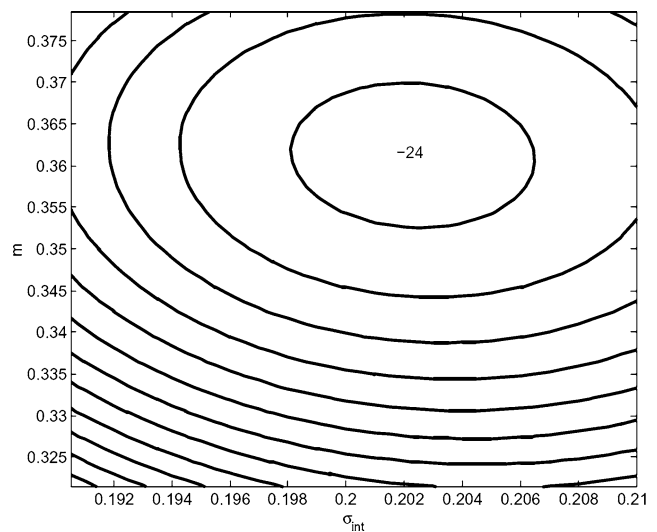

Fig. 10 The likelihood function in the (m, σ_{int}) plane for $\Omega_M = 0.2975$, $\Omega_\Lambda = 0.70$ and $\Omega_k = 0$ for the Amati relation obtained from the *Swift*/BAT data. The *contours* represent the same value of the function $-\ln \mathcal{L}$ obtained for different pairs (m, σ_{int}). For the innermost contour, $-\ln \mathcal{L} = -24$, and for each next one, 0.02 is added

In Fig. 8, we plot the values of the function $-\ln \mathcal{L}$ in the (m, Ω_M) plane for a constant value of $\sigma_{int} = 0.2$. Each contour is characterized by one value of $-\ln \mathcal{L}$. We note that the best value for $-\ln \mathcal{L}$ corresponds to low values of $\Omega_M \leq$.

In Fig. 9, we plot the values of the function $-\ln \mathcal{L}$ in the (σ_{int}, Ω_M) plane for a slope value of $m = 0.37$. Each contour is characterized by one value of $-\ln \mathcal{L}$. We note that the best value for $-\ln \mathcal{L}$ corresponds to low values of $\Omega_M \leq 0.3$.

In Fig. 10, we plot values of the function $-\ln \mathcal{L}$ in the plane (m, σ_{int}), assuming a constant value of $\Omega_M = 0.3$. Each contour represents one value of $-\ln \mathcal{L}$. We note that the best fit is for $-\ln \mathcal{L} = -24$, which corresponds to a slope $m = 0.360 \pm 0.005$ and $\sigma_{int} = 0.202 \pm 0.004$. The intercept of the best fit is -17 ± 1.

Next, we attempt to constrain the cosmological parameters Ω_Λ and Ω_M, using the Amati relation as studied in our previous work (Zitouni et al. 2014), but in any universe (cosmological topology), that is assuming a curvature constant $\Omega_k = 1 - \Omega_M - \Omega_\Lambda$. We first determine the best values of $L = -\ln \mathcal{L}$, which correspond to the parameters (m, q) of a straight line. In this case we vary Ω_M between 0 and 1.2 and Ω_Λ between 0 and 1, independently. Our results are

shown graphically in Fig. 11 and (with more detail) in tabular form in Table 4. The best values of the function $-\ln \mathcal{L}$ correspond to small values of Ω_M and large values of Ω_Λ. In other words, the statistical method that is used tends to favor a universe dominated by dark energy if the Amati relation is correct, and not simply due to a selection effect (Nakar and Piran 2005). For example, for $\Omega_M = 0.0175$; $\Omega_\Lambda = 0.975$ we get $m = 0.3275 \pm 0.0025$ and $\sigma_{int} = 0.193 \pm 0.0015$ with rather high precision.
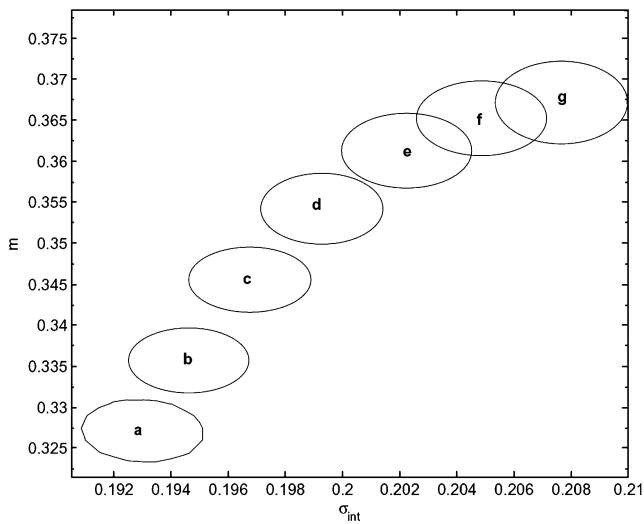
Fig. 11 The likelihood fonction in the (m, σ_{int}) plane for different values of Ω_M and Ω_Λ using the Amati relation with *Swift*/BAT data for 27 GRBs (Zitouni et al. 2014). The contours represent the values of the $-\ln\mathcal{L}$ function. For more information, please refer to Table 4

Table 4 Values of the slope m and σ_{int} for various values of Ω_M and Ω_Λ. a, b and f represent the contours of Fig. 11

	Ω_M	Ω_Λ	$-\ln\mathcal{L}$
a	0.0175	0.975	-25.03
b	0.0525	0.975	-24.83
c	0.0875	0.925	-24.58
d	0.1575	0.80	-24.32
e	0.2975	0.70	-24.00
f	0.50	0.50	-23.74
g	0.10	0.997	-23.47

In Fig. 12 we show the best values of the function $-\ln\mathcal{L}$ plotted in an Ω_M, Ω_Λ plane diagram. On the same figure we present the contours of the values obtained by our methods for determining the cosmological parameters using the SNe Ia data. We note that it is difficult to constrain the cosmological constants using GRB correlation relations without making use of supernovae data (Riess et al. 2004; Xu et al. 2005). The methods agree for values centered around $\Omega_M = 0.3$ and $\Omega_\Lambda = 0.7$. We wish to stress the fact that we did not use the Amati relation as found for the specific values of $\Omega_M = 0.3$ and $\Omega_\Lambda = 0.7$ in order to constrain these same parameters; that would be falling into the circularity trap (Ghirlanda et al. 2004; Dai et al. 2004).

By inverting the Amati relation and taking $E_{p,i}$ as an independent variable and E_{iso} as a variable which depends on the cosmological parameters, we obtain the results shown in Fig. 13. This second Amati relation is expressed by $\log E_{iso} = m \log E_{p,i} + q$. In this case, the corresponding values of m, q, σ_{int}, and $-\ln\mathcal{L}$ are given in Table 5. We

Table 5 Best values obtained for the parameters of the second Amati relation using the likelihood method for various values of Ω_M and Ω_Λ. Data used here consist of 27 GRBs, taken from our previous work (Zitouni et al. 2014)

m	q	σ_{int}	$-\ln\mathcal{L}$
1.15	49.72	0.4216	-3.79
1.20	49.71	0.4240	-3.90
1.25	49.65	0.4264	-3.94
1.30	49.75	0.4328	-3.87
1.45	49.56	0.4512	-3.30
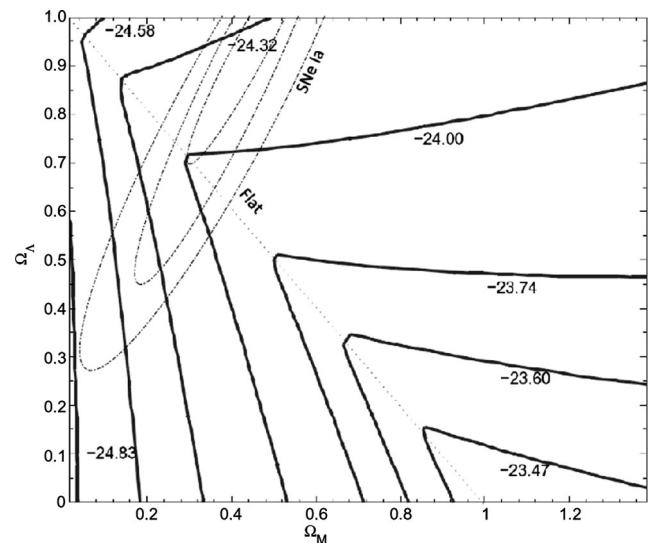
Fig. 12 The contours of the function $-\ln(\mathcal{L})$ in the Ω_M, Ω_Λ plane, using the Amati relation obtained from the *Swift*/BAT data. The *contours* represent the same values of the function $-\ln\mathcal{L}$ corresponding to m and σ_{int} given in Table 6. The *dotted-line contours* are the results obtained using the methods based on SNe Ia

note that the values of σ_{int} and $-\ln\mathcal{L}$ are larger than those obtained with the first Amati relation. On the other hand, we note that with the inverse Amati relation, the likelihood methods tends to prefer cosmological parameters that converge toward $\Omega_M = 0.28$ and $\Omega_\Lambda = 0.725$.

Our approach was rather to find the best values of the cosmological parameters that correspond to the minimum value(s) of $(-\ln\mathcal{L})$ and to then infer the correlation constants m and q. This method, however, is very sensitive to the dispersion of the data. It allows one to converge on rather precise values if the data have been obtained with high precision. This procedure also allows one to verify a correlation relation by comparing with the results obtained through other methods and data (WMAP: the Wilkinson Microwave Anisotropy Probe, SN Ia).
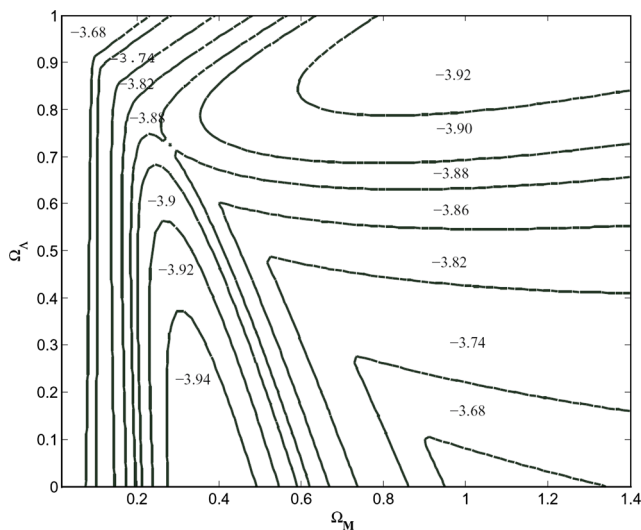
Fig. 13 The contours of the function $-\ln(\mathcal{L})$ in the Ω_M, Ω_Λ plane, using the inverted Amati relation obtained from the *Swift*/BAT data. The *contours* represent the same values of the function $-\ln\mathcal{L}$ corresponding to m and σ_{int} given in Table 5. The *meeting point of the contours* correspond $\Omega_M = 0.28$ and $\Omega_\Lambda = 0.725$

7.2 Usage of the Dainotti relation

We have also attempted to use the correlation that was obtained above between the break time T_a seen in the X-ray afterglow's time evolution and the luminosity L_X at that instant. For that we used the 73 bursts that we had selected. We chose this correlation because it relates an observed quantity to one which is calculated in terms of the cosmological parameters. That relation is expressed by Eq. (13) and applies to a flat universe with ($\Omega_k = 0$, $\Omega_\Lambda = 0.7$, $\Omega_M = 0.3$, $H_0 = 70\ \mathrm{km\,s^{-1}\,Mpc^{-1}}$). In what follows we study that relation for a more general case.

Before applying our method, let us explain what we would like to accomplish, assuming the ideal case in which our data do not suffer from any dispersion. In Fig. 14, we present the case where $\Omega_M = 0.3$. We note that our method does converge toward ($\Omega_M = 0.3$, $\Omega_\Lambda = 0.7$). This is a way to check the validity of our method and the impact of the dispersion of data on our results.

In Fig. 15 we use the Dainotti correlation relation $L_X(T_a) - T_a$ to constrain (Ω_M, Ω_Λ) in any type of universe. We present the results as contours of specific values of $-\ln\mathcal{L}$. We note that the best values of this function, that is the minima of the function, are obtained for $\Omega_\Lambda \rightarrow 0$ and $\Omega_M \rightarrow 1$. In other words, Dainotti correlation relation works best in a universe dominated by matter. This result is opposite to what was obtained with the Amati relation. On the other hand, if we include the results obtained using supernovae, we obtain the same earlier results, namely values closer to ($\Omega_M = 0.3$, $\Omega_\Lambda = 0.7$) for a flat universe.

In Fig. 16 we show the contours for the best values of the function $-\ln\mathcal{L}$ in the (m, σ_{int}) plane for different values of
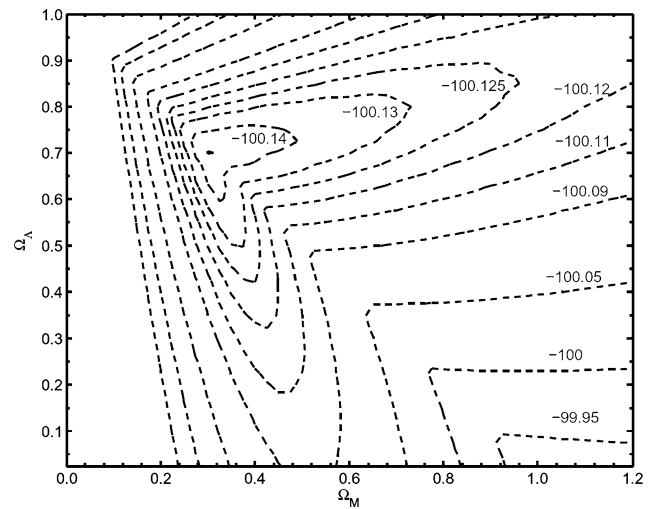

Fig. 14 The function $-\ln\mathcal{L}$ in the (Ω_M, Ω_Λ) plane for Dainotti correlation relation between the X-ray luminosity X at T_a as a function of the break time after the temporal plateau. In the ideal case, we have used a straight line ($\log\frac{T_a}{1+z} = -0.46\log F_x(T_a) + 25.2$)
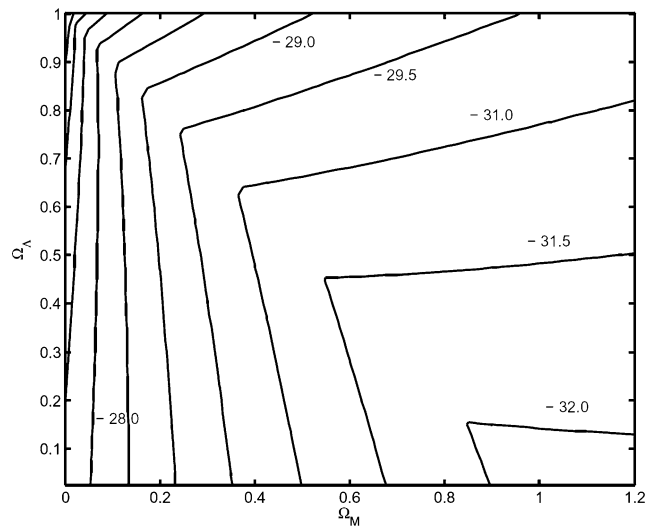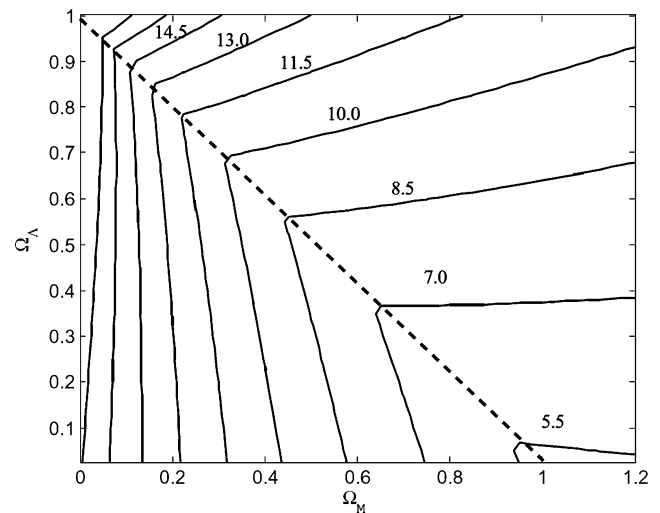

Fig. 15 The function $-\ln\mathcal{L}$ in the (Ω_M, Ω_Λ) plane using the Dainotti correlation relation between $L_X(T_a)$ and T_a

the pair (Ω_M, Ω_Λ). Information for each contour is given in Table 6. For example, for contour B, corresponding to ($\Omega_M = 0.3$, $\Omega_\Lambda = 0.7$), we get $m = -0.462 \pm 0.014$ and $\sigma_{int} = 0.288 \pm 0.012$.

In Fig. 17 we show the obtained values of (m, σ_{int}) starting from a flat space characterized by $\Omega_M = 0.3$. We here note the ability of the likelihood method to converge to the best values of m and σ_{int}.

When we express the Dainotti relation by taking $Ta/(1+z)$ as an independent variable and L_X as a variable that depends on cosmological parameters, we obtain the results shown in Fig. 18. The relation that is represented there is $\log L_X = m\ \log(T_a/(1+z)) + q$, and we refer to it as the

Table 6 Values for the slope m and σ_{int} for different values of Ω_M and Ω_Λ. A and E represent the contours in Fig. 16

	Ω_M	Ω_Λ	$-\ln\mathcal{L}$
A	0.90	0.01	−32.02
B	0.50	0.50	−31.34
C	0.30	0.70	−30.72
D	0.10	0.90	−29.40
E	0.00	0.025	−28.55
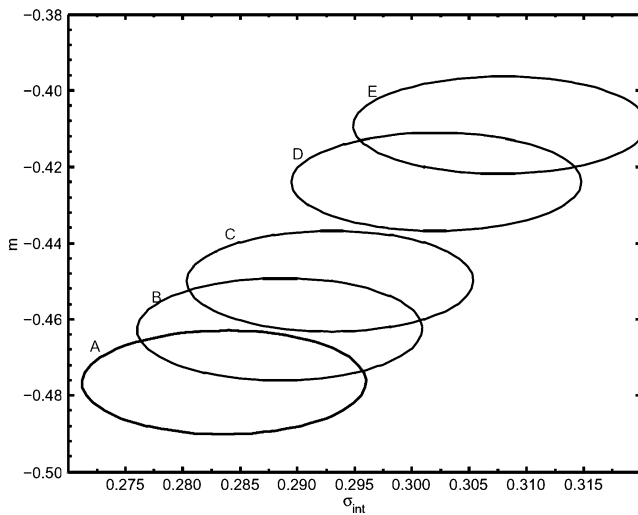
Fig. 16 The likelihood function in the (m, σ_{int}) plane for different values of Ω_M and Ω_Λ using the Dainotti correlation between $L_X(T_a)$ and T_a we obtained from the *Swift*/BAT data for 70 GRBs. The *contours* represent the values of the function $-\ln\mathcal{L}$. Further information on A and E, please refer to Table 6

Table 7 Best values obtained for the parameters of the second Dainotti relation using the likelihood method for various values of Ω_M and Ω_Λ

m	q	σ_{int}	$-\ln\mathcal{L}$
−1.29	51.38	0.505	5.43
−1.30	51.45	0.510	6.05
−1.31	51.53	0.520	7.07
−1.33	51.71	0.535	9.05
−1.35	51.89	0.555	11.05
−1.38	52.14	0.590	14.09
−1.41	52.37	0.615	17.21

'second Dainotti relation' to distinguish it from the first one referred to earlier. In this case, the corresponding values of m, q, σ_{int}, and $-\ln\mathcal{L}$ are given in Table 7. We note that the values of σ_{int} and $-\ln\mathcal{L}$ are larger than those obtained with the first Dainotti relation while showing the same general trend.
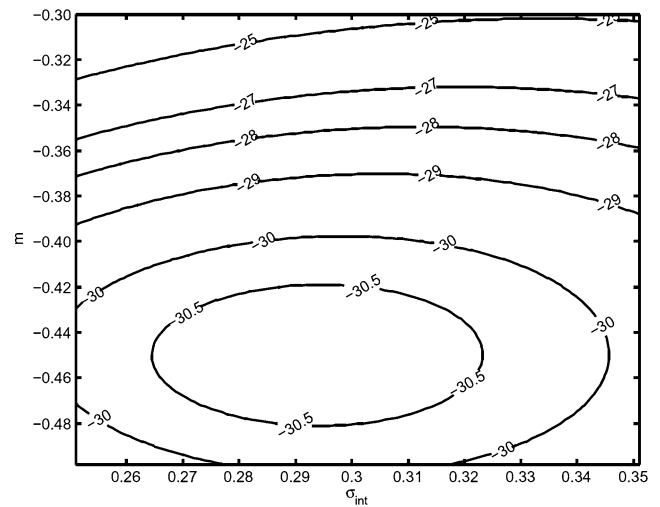
Fig. 17 The function $-\ln\mathcal{L}$ in the (σ_{int}, m) plane for Dainotti correlation between the X-ray luminosity and T_a as a function of the break time after the temporal plateau. $\Omega_M = 0.3$

Fig. 18 The contours of the function $-\ln(\mathcal{L})$ in the Ω_M, Ω_Λ plane, using the second Dainotti relation obtained from the *Swift*/BAT data. The *contours* represent the same values of the function $-\ln\mathcal{L}$ corresponding to m and σ_{int} given in Table 7

8 Discussion

This study was conducted to try to determine the cosmological parameters Ω_Λ and Ω_M by using two correlation relations: the Amati relation between E_p and E_{iso} and a Dainotti relation between T_a and $L_X(T_a)$, which we presented in the previous sections. The Amati relation has been widely used to this aim (Dai et al. 2004; Amati et al. 2008; Kodama et al. 2008; Wei et al. 2013; Wang et al. 2016). However, this relation was inferred by assuming a flat universe with $\Omega_M = 0.3$, while some of the above-mentioned works use it as is and at the same time try to determine the cosmological parameters, which raises the issue of the cir-

culularity problem. Other works use a calibration based on the results from SN Ia for redshifts $z < 1.414$ (Wang et al. 2015, 2016), which we view as a good approach (associating the results from SNe Ia with data from GRBs).

In the present work, we have tried to constrain the cosmological parameters using the two Amati relations relation but without setting a priori values of the slope and intercept parameters m and q. The best values are those that minimize the function $L = -\ln \mathcal{L}$. This requirement leads to a set of values for Ω_M et Ω_Λ that produce contours in the plane of those cosmological variables/parameters. We find that the first Amati relation tends to favor values of $\Omega_M \to 0$ and $\Omega_\Lambda \to 1$. To relate our result with that obtained from SNe Ia, we have graphically superposed the two. On the other hand, the second Amati relation favors values of the cosmological parameters that tend to converge toward $\Omega_M = 0.28$ and $\Omega_\Lambda = 0.725$ in the best cases.

The second relation, Dainotti relation, which we confirmed from *Swift*/XRT data is between the breaking time T_a in the time profile of the X-ray flux and the luminosity $L_X(T_a)$. However, it is characterized by large dispersions of the data points around the interpolation (straight) line. For the two versions of the Dainotti relation, our statistical analysis tends to favor values of $\Omega_M \to 1$ and $\Omega_\Lambda \to 0$. By numerically reducing the dispersion of the data, the results are greatly improved and converge to a set of values of the cosmological parameters close to what is obtained by other methods

By numerically reducing the dispersion of the data, the results are greatly improved and converge to a set of values of the cosmological parameters close to what is obtained by other methods; the results are also close to those presented in Fig. 14, which seems to confirm the need for "clean" data with minimal data dispersion around the straight line. We note that the Dainotti correlation has been used by several authors in an effort to constrain the cosmological parameters (Cardone et al. 2009, 2010; Dainotti et al. 2013b; Petrosian et al. 2015).

9 Conclusion

Gamma-ray bursts hold great potential as cosmological probes. This fact, however, has not yet been fully utilized, mainly because GRBs are not standard candles and partly because it has been difficult to construct plots between GRB characteristics that do not show too much scatter. The discovery and calibration of several luminosity and energy correlations has ushered in a new period of investigation in which GRBs are finally beginning to prove their worth as cosmological probes. In this paper, we tried to put limits on the values of q and m by utilizing the well-known Amati relation and one that was obtained by Dainotti et al. (2008)

from GRB data, namely a correlation between the X-ray burst luminosity L_X and the break time T_a in the X-ray flux's time profile, a correlation that we confirmed with our sample. The latter relation suffers from wide scatter, but we were able to narrow this scatter using numerical techniques. This enabled us to get reasonable values for Ω_Λ and Ω_M that are consistent with those obtained via other methods. A few general conclusions may be drawn from this work:

1. despite the wealth of GRB data that we now have (from *Swift*, Fermi, and others), the data that is plotted in the "standard" ways (luminosity vs. time, luminosity vs energy in various bands, etc.) still shows much scatter, at least for cosmological research purposes. Either we need more data in different energy bands or we are missing some insights as to how to relate various quantities.
2. The correlation that we have confirmed(between L_X and T_a), while far from perfect, shows that interesting perspectives can still be obtained by looking at the data from different angles.
3. Diversifying analysis approaches (maximum likelihood, chi-square minimization, iterative convergence, etc.) can yield interesting results that one may compare and contrast to reach the most robust conclusions.
4. For cosmological studies, while GRBs may certainly represent an important new angle from which to approach the determination of various parameters, combining quantities and results from different methods (SN Ia supernovae, Cosmic Microwave Background, Gamma Ray Bursts) and ensuring consistency across the board appears to be not only the best general approach but perhaps an absolutely necessary one.

In the future, we hope to pursue this new, promising avenue along the lines of the above general conclusions, in the aim of placing more stringent limits on the values of cosmological parameters, particularly by using larger data sets and GRB characteristics (energies and fluxes from various intervals and bands), which may aid in reducing the scatter in the correlation relations and thus in obtaining more precise results.

References

Amati, L.: Chin. J. Astron. Astrophys. Suppl. **3**, 455 (2003). astro-ph/0405318

Amati, L.: Mon. Not. R. Astron. Soc. **372**, 233 (2006). doi:10.1111/j.1365-2966.2006.10840.x

Amati, L., Della Valle, M.: Int. J. Mod. Phys. D **22**, 1330028 (2013). 1310.3141. doi:10.1142/S0218271813300280

Amati, L., Frontera, F., Guidorzi, C.: Astron. Astrophys. **508**, 173 (2009). 0907.0384. doi:10.1051/0004-6361/200912788

Amati, L., Frontera, F., Tavani, M., Zand, J.J.M., Antonelli, A., Costa, E., Feroci, M., Guidorzi, C., Heise, J., Masetti, N., Montanari, E., Nicastro, L., Palazzi, E., Pian, E., Piro, L., Soffitta, P.: Astron. Astrophys. **390**, 81 (2002). doi:10.1051/0004-6361:20020722

Amati, L., Guidorzi, C., Frontera, F., Della Valle, M., Finelli, F., Landi, R., Montanari, E.: Mon. Not. R. Astron. Soc. **391**, 577 (2008). 0805.0377. doi:10.1111/j.1365-2966.2008.13943.x

Azzam, W.J., Alothman, M.J.: Adv. Space Res. **38**, 1303 (2006a). doi:10.1016/j.asr.2004.12.019

Azzam, W.J., Alothman, M.J.: Nuovo Cimento B **121**, 1431 (2006b). doi:10.1393/ncb/i2007-10270-5

Cardone, V.F., Capozziello, S., Dainotti, M.G.: Mon. Not. R. Astron. Soc. **400**, 775 (2009). 0901.3194

Cardone, V.F., Perillo, M., Capozziello, S.: Mon. Not. R. Astron. Soc. **417**, 1672 (2011). 1105.1122

Cardone, V.F., Dainotti, M.G., Capozziello, S., Willingale, R.: Mon. Not. R. Astron. Soc. **408**, 1181 (2010). 1005.0122. doi:10.1111/j.1365-2966.2010.17197.x

Coward, D.: New Astron. Rev. **51**, 539 (2007). astro-ph/0702704. doi:10.1016/j.newar.2007.03.003

D'Agostini, G.: physics/0511182 (2005)

Dai, Z.G., Liang, E.W., Xu, D.: Astrophys. J. Lett. **612**, 101 (2004). astro-ph/0407497. doi:10.1086/424694

Daigne, F., Mochkovitch, R.: Astron. Astrophys. **465**, 1 (2007). 0707.0931. doi:10.1051/0004-6361:20066080

Dainotti, M.G., Cardone, V.F., Capozziello, S.: Mon. Not. R. Astron. Soc. **391**, 79 (2008). 0809.1389

Dainotti, M.G., Ostrowski, M., Willingale, R.: Mon. Not. R. Astron. Soc. **418**, 2202 (2011). 1103.1138. doi:10.1111/j.1365-2966.2011.19433.x

Dainotti, M.G., Willingale, R., Capozziello, S., Fabrizio Cardone, V., Ostrowski, M.: Astrophys. J. Lett. **722**, 215 (2010). 1009.1663. doi:10.1088/2041-8205/722/2/L215

Dainotti, M.G., Petrosian, V., Singal, J., Ostrowski, M.: Astrophys. J. **774**, 157 (2013a). 1307.7297

Dainotti, M.G., Cardone, V.F., Piedipalumbo, E., Capozziello, S.: Mon. Not. R. Astron. Soc. **436**, 82 (2013b). 1308.1918. doi:10.1093/mnras/stt1516

Dainotti, M.G., Del Vecchio, R., Shigehiro, N., Capozziello, S.: Astrophys. J. **800**, 31 (2015a). 1412.3969

Dainotti, M., Petrosian, V., Willingale, R., O'Brien, P., Ostrowski, M., Nagataki, S.: Mon. Not. R. Astron. Soc. **451**, 3898 (2015b). 1506.00702. doi:10.1093/mnras/stv1229

Dainotti, M., Postnikov, S., Hernandez, X., Ostrowski, M.: 1604.06840 (2016)

D'Avanzo, P., Salvaterra, R., Sbarufatti, B., Nava, L., Melandri, A., Bernardini, M.G., Campana, S., Covino, S., Fugazza, D., Ghirlanda, G., Ghisellini, G., Parola, V.L., Perri, M., Vergani, S.D., Tagliaferri, G.: Mon. Not. R. Astron. Soc. **425**, 506 (2012). 1206.2357. doi:10.1111/j.1365-2966.2012.21489.x

Dermer, C.D.: Astrophys. Space Sci. **309**, 127 (2007). astro-ph/0610195. doi:10.1007/s10509-007-9417-8

Evans, P.A., Beardmore, A.P., Page, K.L., Osborne, J.P., O'Brien, P.T., Willingale, R., Starling, R.L.C., Burrows, D.N., Godet, O., Vetere, L., Racusin, J., Goad, M.R., Wiersema, K., Angelini, L., Capalbi, M., Chincarini, G., Gehrels, N., Kennea, J.A., Margutti, R., Morris, D.C., Mountford, C.J., Pagani, C., Perri, M., Romano, P., Tanvir, N.: Mon. Not. R. Astron. Soc. **397**, 1177 (2009). 0812.3662. doi:10.1111/j.1365-2966.2009.14913.x

Fenimore, E.E., Ramirez-Ruiz, E.: astro-ph/0004176 (2000)

Ghirlanda, G., Ghisellini, G., Lazzati, D.: Astrophys. J. **616**, 331 (2004). doi:10.1086/424913

Ghirlanda, G., Nava, L., Ghisellini, G.: Astron. Astrophys. **511**, 43 (2010). 0908.2807. doi:10.1051/0004-6361/200913134

Ghirlanda, G., Ghisellini, G., Lazzati, D., Firmani, C.: Astrophys. J. Lett. **613**, 13 (2004). astro-ph/0408350. doi:10.1086/424915

Ghirlanda, G., Ghisellini, G., Firmani, C., Nava, L., Tavecchio, F., Lazzati, D.: Astron. Astrophys. **452**, 839 (2006). astro-ph/0511559. doi:10.1051/0004-6361:20054544

Ghirlanda, G., Salvaterra, R., Ghisellini, G., Mereghetti, S., Tagliaferri, G., Campana, S., Osborne, J.P., O'Brien, P., Tanvir, N., Willingale, D., Amati, L., Basa, S., Bernardini, M.G., Burlon, D., Covino, S., D'Avanzo, P., Frontera, F., Götz, D., Melandri, A., Nava, L., Piro, L., Vergani, S.D.: Mon. Not. R. Astron. Soc. **448**, 2514 (2015). 1502.02676. doi:10.1093/mnras/stv183

Hopkins, A.M., Beacom, J.F.: Astrophys. J. **651**, 142 (2006). astro-ph/0601463. doi:10.1086/506610

Jakobsson, P., Levan, A., Fynbo, J.P.U., Priddey, R., Hjorth, J., Tanvir, N., Watson, D., Jensen, B.L., Sollerman, J., Natarajan, P., Gorosabel, J., Castro Cerón, J.M., Pedersen, K., Pursimo, T., Árnadóttir, A.S., Castro-Tirado, A.J., Davis, C.J., Deeg, H.J., Fiuza, D.A., Mikolaitis, S., Sousa, S.G.: Astron. Astrophys. **447**, 897 (2006). astro-ph/0509888. doi:10.1051/0004-6361:20054287

Kistler, M.D., Yüksel, H., Beacom, J.F., Stanek, K.Z.: Astrophys. J. Lett. **673**, 119 (2008). 0709.0381

Kodama, Y., Yonetoku, D., Murakami, T., Tanabe, S., Tsutsui, R., Nakamura, T.: Mon. Not. R. Astron. Soc. **391**, 1 (2008). 0802.3428

Liang, E., Zhang, B.: Astrophys. J. **633**, 611 (2005). astro-ph/504404. doi:10.1086/491594

Mao, J.: Astrophys. J. **717**, 140 (2010). 1005.1876

Mao, S., Mo, H.J.: Astron. Astrophys. **339**, 1 (1998). astro-ph/9808342

Margutti, R., Zaninoni, E., Bernardini, M.G., Chincarini, G., Pasotti, F., Guidorzi, C., Angelini, L., Burrows, D.N., Capalbi, M., Evans, P.A., Gehrels, N., Kennea, J., Mangano, V., Moretti, A., Nousek, J., Osborne, J.P., Page, K.L., Perri, M., Racusin, J., Romano, P., Sbarufatti, B., Stafford, S., Stamatikos, M.: Mon. Not. R. Astron. Soc. **428**, 729 (2013). 1203.1059. doi:10.1093/mnras/sts066

Martin, B.: Statistics for Physical Sciences: An Introduction. Academic Press, London (2012)

Nakar, E., Piran, T.: Mon. Not. R. Astron. Soc. **360**, 73 (2005). astro-ph/0412232

Natarajan, P., Albanna, B., Hjorth, J., Ramirez-Ruiz, E., Tanvir, N., Wijers, R.: Mon. Not. R. Astron. Soc. **364**, 8 (2005). astro-ph/0505496. doi:10.1111/j.1745-3933.2005.00094.x

Norris, J.P., Marani, G.F., Bonnell, J.T.: Astrophys. J. **534**, 248 (2000). astro-ph/9903233. doi:10.1086/308725

Petrosian, V., Kitanidis, E., Kocevski, D.: Astrophys. J. **806**, 44 (2015). 1504.01414

Porciani, C., Madau, P.: Astrophys. J. **548**, 522 (2001). astro-ph/0008294. doi:10.1086/319027

Riess, A.G., Strolger, L.-G., Tonry, J., Casertano, S., Ferguson, H.C., Mobasher, B., Challis, P., Filippenko, A.V., Jha, S., Li, W., Chornock, R., Kirshner, R.P., Leibundgut, B., Dickinson, M., Livio, M., Giavalisco, M., Steidel, C.C., Benítez, T., Tsvetanov, Z.: Astrophys. J. **607**, 665 (2004). astro-ph/0402512. doi:10.1086/383612

Sakamoto, T., Barthelmy, S.D., Baumgartner, W.H., Cummings, J.R., Fenimore, E.E., Gehrels, N., Krimm, H.A., Markwardt, C.B., Palmer, D.M., Parsons, A.M., Sato, G., Stamatikos, M., Tueller, J., Ukwatta, T.N., Zhang, B.: Astrophys. J. Suppl. Ser. **195**, 2 (2011). 1104.4689. doi:10.1088/0067-0049/195/1/2

Saporta, G.: Probabilitès, Analyse des Donnèes et Statistique, 2nd edn. Editions Technip, Paris (2011)

Schaefer, B.E.: Astrophys. J. Lett. **583**, 67 (2003). astro-ph/0212445. doi:10.1086/368104

Schaefer, B.E.: Astrophys. J. **660**, 16 (2007). astro-ph/0612285. doi:10.1086/511742

Sultana, J., Kazanas, D., Fukumura, K.: Astrophys. J. **758**, 32 (2012). 1208.1680. doi:10.1088/0004-637X/758/1/32

Totani, T.: Astrophys. J. Lett. **486**, 71 (1997). astro-ph/9707051. doi:10.1086/310853

van Eerten, H.J.: Mon. Not. R. Astron. Soc. **445**, 2414 (2014). 1404.0283. doi:10.1093/mnras/stu1921

Wang, F.Y., Dai, Z.G., Liang, E.W.: New Astron. Rev. **67**, 1 (2015). 1504.00735. doi:10.1016/j.newar.2015.03.001

Wang, J.S., Wang, F.Y., Cheng, K.S., Dai, Z.G.: Astron. Astrophys. **585**, 68 (2016). 1509.08558. doi:10.1051/0004-6361/201526485

Wei, J.-J., Wu, X.-F., Melia, F.: Astrophys. J. **772**, 43 (2013). 1301.0894. doi:10.1088/0004-637X/772/1/43

Wijers, R.A.M.J., Bloom, J.S., Bagla, J.S., Natarajan, P.: Mon. Not. R. Astron. Soc. **294**, 13 (1998). astro-ph/9708183. doi:10.1046/j.1365-8711.1998.01328.x

Willingale, R., O'Brien, P.T., Osborne, J.P., Godet, O., Page, K.L., Goad, M.R., Burrows, D.N., Zhang, B., Rol, E., Gehrels, N., Chincarini, G.: Astrophys. J. **662**, 1093 (2007). astro-ph/0612031. doi:10.1086/517989

Xu, D., Dai, Z.G., Liang, E.W.: Astrophys. J. **633**, 603 (2005). astro-ph/0501458. doi:10.1086/466509

Yonetoku, D., Murakami, T., Nakamura, T., Yamazaki, R., Inoue, A.K., Ioka, K.: Astrophys. J. **609**, 935 (2004). arXiv:astro-ph/0309217. doi:10.1086/421285

Yüksel, H., Kistler, M.D.: Phys. Rev. D **75**(8), 083004 (2007). astro-ph/0610481

Zaninoni, E., Bernardini, M.G., Margutti, R., Amati, L.: Mon. Not. R. Astron. Soc. **455**, 1375 (2016). 1510.05673

Zitouni, H., Guessoum, N., Azzam, W.J.: Astrophys. Space Sci. **351**, 267 (2014). doi:10.1007/s10509-014-1839-5